

Carbon sequestration potential of Mg carbonate and silicate biomineralization in the presence of cyanobacterium *Synechococcus*

Céline Lamérand^a, Liudmila S. Shirokova^{a,b}, Pascale Bénézech^a, Jean-Luc Rols^c, Oleg S. Pokrovsky^{a,d,*}

^a Géosciences Environnement Toulouse, GET – CNRS – IRD – OMP – Université de Toulouse, 14, Avenue Edouard Belin, 31400 Toulouse, France

^b N. Laverov Federal Center for Integrated Arctic Research of the Ural Branch of the Russian Academy of Sciences (FECLAR UrB RAS), Arkhangelsk, Russia

^c Laboratoire écologie fonctionnelle et environnement, Université de Toulouse, CNRS, INP, Université Toulouse 3 – Paul Sabatier (UPS), Toulouse, France

^d BIO-GEO-CLIM Laboratory, Tomsk State University, Tomsk, Russia

ARTICLE INFO

Editor: Hailiang Dong

ABSTRACT

Bacterially-induced sequestration of atmospheric CO₂ is at the forefront of geomicrobiological research due to high potential of this process in the mitigation of climate warming. Cyanobacteria have been known to form stromatolites since the Precambrian and could be used to enhance this process by sequestering carbon via the biomineralization of Mg and Ca carbonates. Currently, olivine (MgSiO₄) is considered as one of the most efficient silicate minerals suitable for CO₂ capture in the form of secondary Mg carbonates. However, the role of dissolved Si on the efficiency of biomineralization is not sufficiently well understood. The present study intended to reproduce in the laboratory the processes of biomineralization by *Synechococcus* sp. cyanobacteria extracted from modern stromatolites in a carbonate- and Mg-bearing medium containing various Si concentrations, in order to characterize the rates and stoichiometry of reactions as well as mineralogical nature of precipitates. The results demonstrated the dominant role of cyanobacterial metabolism in the precipitation of carbonate minerals by increasing the pH of the medium via photosynthesis and providing a template in the form of cell walls and their EPS for mineral nucleation. Transmission electron microscopy and other microscopic and spectroscopic observations and analyses identified magnesium carbonates and silicates, such as nesquehonite (MgCO₃·3H₂O) and/or hydromagnesite (Mg₅(CO₃)₄(OH)₂·4(H₂O) together with amorphous analogue of sepiolite (Mg₄Si₆O₁₅(OH)₂·6H₂O) as dominant precipitated minerals. Apparent inorganic C precipitation rates were not affected by the concentration of Mg and Si in the initial solution. However, the carbon sequestration potential was 20–40% higher in the presence of Si. Overall, the experimental approach developed in this study allows efficient reproduction of combined Mg hydroxy-carbonate and hydrous silicate precipitation under cyanobacterial activity and helps to constrain optimal conditions of cyanobacteria-induced CO₂ sequestration.

1. Introduction

One of the considered options to decrease the rising CO₂ concentration in the atmosphere is to capture the CO₂ and store it in geological reservoirs (Matter et al., 2009; Matter and Kelemen, 2009; Sun et al., 2020). An alternative solution is the mineralization of CO₂ into mafic and/or ultramafic rocks (peridotites, serpentinites) composed of silicates of magnesium, iron and calcium, which allows a thermodynamic stable and safe storage (Oelkers et al., 2008; Matter and Kelemen, 2009; Bénézech et al., 2014). Indeed, CO₂ can react with these minerals

producing Ca, Mg and Fe cations forming carbonated minerals, thus reproducing natural biogeochemical carbon (C) cycle of weathering and carbonate mineral precipitation.

Numerous experimental and field studies are devoted to the mechanisms of serpentinization and carbonatation of ultramafic rocks, all useful in the context of a possible industrial storage of CO₂ and its valorization (see Kelemen et al., 2011). In these studies, the forsteritic olivine (Mg,Fe)₂SiO₄ is generally used as representative mineral of these rocks because it plays an important role in the mechanisms of geological CO₂ sequestration via carbonatation, both in abiotic (Sissmann et al.,

* Corresponding author at: Géosciences Environnement Toulouse, GET – CNRS – IRD – OMP – Université de Toulouse, 14, Avenue Edouard Belin, 31400 Toulouse, France.

E-mail address: oleg.pokrovsky@get.omp.eu (O.S. Pokrovsky).

<https://doi.org/10.1016/j.chemgeo.2022.120854>

Received 14 December 2021; Received in revised form 14 February 2022; Accepted 4 April 2022

Available online 7 April 2022

0009-2541/© 2022 Elsevier B.V. All rights reserved.

2013; Peuble et al., 2015) and biotic (Power et al., 2009; Shirokova et al., 2013; Bundeleva et al., 2014a, 2014b; McCutcheon et al., 2014; Martinez et al., 2016) systems. Microorganisms are capable of C sequestration through mineral trapping via precipitation of dissolved CO₂, usually in the form of carbonate minerals such as CaCO₃ (Mittel et al., 2010; Dhimi et al., 2014; Pan et al., 2018; Zhu et al., 2015, 2018; Zhuang et al., 2018; Saneiyani et al., 2019; Naveed et al., 2020; He et al., 2022) thus providing durable carbon immobilization over a geological time scale (Pires et al., 2012).

Among aquatic microorganisms, cyanobacteria play a central role in the bio-precipitation of carbonate minerals. Being modern representatives of the first living organisms on the Earth, these bacteria have been forming carbonated rocks, called stromatolites, in shallow marine or lacustrine environments (a few dozen meters), the oldest of which situated in south-west Greenland are aged of 3.7 Ga (Nutman et al., 2016). The potential of calcifying cyanobacteria for geological CO₂ storage was demonstrated by Jansson and Northen (2010). Some studies showed the precipitation of magnesian carbonates following the dissolution of olivine in the presence of green algae consortium (Power et al., 2011), cyanobacteria *Synechococcus* sp. (Martinez et al., 2016) or bacterial consortium (Lamérand et al., 2020). The precipitation of hydrated magnesian carbonates was accelerated in the presence of cyanobacteria *Gloeocapsa* sp., via the increase of pH in bicarbonate-bearing solutions under conditions similar to those of the natural environment (Mavromatis et al., 2012). For example, in the alkaline Salda Lake (Turkey), cyanobacteria *Synechococcus* sp. form stromatolites composed of hydrated magnesian carbonates such as hydromagnesite (Mg₅(CO₃)₄(OH)₂·4H₂O), by locally increasing the pH and providing the nucleation sites on the surface of cells, allowing the formation of minerals (Shirokova et al., 2013). In this lake, underground springs enriched with Mg due to dissolution of peridotites at the lake watershed, form waters rich in Mg and Si (Shirokova et al., 2012).

Most of these laboratory studies of the formation of Mg carbonate by cyanobacteria were performed with solely aqueous Mg and carbonate in solution, yet the biomineralization of Mg carbonate in the context of CO₂ storage occurs in Si-bearing environments (Lamérand et al., 2020). Over past seven years, sizable efforts have been devoted to laboratory and pilot-scale studies of Mg carbonate biomineralization in cyanobacterial biofilms, in the presence of Mg-rich silicate leaching products (McCutcheon et al., 2014, 2015, 2016, 2017, 2019; McCutcheon and Southam, 2018). However, a possible effect of the presence of aqueous Si on Mg carbonate biomineralization in planktonic cyanobacterial cultures remained very poorly known. It can be anticipated that photosynthetic activity of bacteria in aqueous solutions containing Si and Mg could provoke the formation of both carbonates and magnesium silicates as it is reported from modern stromatolites occurrences (Pace et al., 2016, 2018). In natural settings, magnesian calcite and sepiolite (Mg₄Si₆O₁₅(OH)₂·6H₂O) occur in lakes, subject to massive algae blooms (Barbiero et al., 2002, 2008). Moreover, sepiolite was reported to form under controlled laboratory environment as a precursor of protodolomite (Balan et al., 2018).

Despite numerous studies on Mg carbonate biomineralization via cyanobacteria, the processes leading to the formation of these minerals are not yet fully understood. Two main mechanisms of bio-induced precipitation are currently identified: (i) the increase of pH and saturation state of solution due to the photosynthetic activity of cyanobacteria (Lee et al., 2004; Plee et al., 2010; Ludwig et al., 2005) and (ii) mineral crystallization on exopolymeric substances (EPS) that could decrease the activation barrier via serving as nucleation centers (Dupraz et al., 2009). However, assessing the relative role of each of these mechanisms has not yet fully achieved.

The aims of this study were to 1) acquire new knowledge on the optimal conditions for massive precipitation of Mg carbonate and Mg silicate minerals in the context of CO₂ storage; 2) quantify the rates and characterize the nature of the precipitated solid phases, and 3) identify the mechanisms responsible for the biomineralization processes. For

this, we conducted laboratory experiments with *Synechococcus* sp. cyanobacterium, obtained from alkaline (pH > 9) Salda Lake (Turkey) using carbonate-bearing solution containing different concentrations of Mg and/or Si under different experimental settings, designed to distinguish the effect of solution supersaturation rise, cell surface sites and cell soluble exometabolites. We used a combination of physico-chemical, microscopic and spectroscopic techniques to characterize the formation of organo-mineral solid phases in order to produce a quantitative model of mineral formation in the system Mg - HCO₃ - Si - cyanobacteria at various physicochemical parameters of solution and to estimate the C sequestration potential of this system.

2. Material and methods

2.1. Bacterial strain

Cyanobacteria *Synechococcus* sp. PCC 7942 were isolated from the surface of stromatolites growing in the alkaline, Mg(HCO₃)₂-dominated Salda Lake (Turkey) and used previously in mineral carbonation experiments in pure culture (Shirokova et al., 2013). They were cultured in BG-11 (Sigma-Aldrich C3061) nutrient solution under air bubbling and continuous light to insure most efficient development (Stanier et al., 1979). Before the inoculation of batch reactors, cells were rinsed twice in appropriate fresh culture media (for biotic experiments in BG-11) or sterile 0.1 M NaCl solution (for experiments without nutrients) using centrifugation (~500 mL of solution for 1 g of wet biomass) to remove, as possible, the adsorbed ions and cell exudates from the surface.

2.2. Aqueous solutions

The precipitation of secondary Mg-carbonate and Mg-silicate minerals in the presence of cyanobacteria *Synechococcus* sp. was studied in 10 mM NaHCO₃ aqueous solutions enriched or not with Mg and Si. Aqueous silica was added from a Na₂SiO₃ concentrated solution (Sigma Aldrich, anal. pure) and Mg was added from a MgCl₂ concentrated solution. Various control experiments were performed as similar composition of aqueous solution. The composition of experimental fluids is listed in Table 1.

Table 1

List of conducted experiments, chemical composition of experimental solutions, bacteria status and reactor type. All the experiments were run in the diluted BG-11 (10%) nutrient medium.

Nom	NaHCO ₃ , mM	Mg, mM	Si, mM	Cyanobacteria	Experimental conditions
SiMg	10	5	0.3	1 g _{wet} /L <i>Synechococcus</i> sp.	Aerated, mixed
Mg3	10	10	–	1 g _{wet} /L <i>Synechococcus</i> sp.	Aerated, mixed
SiMg3	10	10	0.4	1 g _{wet} /L <i>Synechococcus</i> sp.	Aerated, mixed
ASiMg	10	5	0.7	Bacteria-free	Aerated, mixed
AMg3	10	10	–	Bacteria-free	Aerated, mixed
ASiMg3	10	10	0.7	Bacteria-free	Aerated, mixed
BSM	10	10	–	1 g _{wet} /L <i>Synechococcus</i> sp.	Aerated, mixed
CSM	10	10	–	1 g _{wet} /L <i>Synechococcus</i> sp.	Aerated, mixed, reactors kept in darkness
DSM	10	10	–	1 g _{wet} /L <i>Synechococcus</i> sp.	Bacteria inside the dialysis bag
SD	10	10	–	1 g _{wet} /L <i>Synechococcus</i> sp.	Bacteria outside the dialysis bag

2.3. Experimental setup

Experimental setup was aimed at testing separately the effect of Mg, HCO_3^- , Si concentration, pH of the aqueous solution, cell photosynthesis, EPS, and the presence of cell surfaces as templates for mineral crystallization. All the experiments were run in duplicates and included: *i*) cyanobacterial suspension in 500 mL polycarbonate Erlenmeyer flasks closed with sterile porous caps (Bio-Silico®) which allowed free atmospheric air exchange (experiments Mg3, SiMg3, SiMg), *ii*) cyanobacteria enclosed into a dialysis bag (pore size 6–8 kDa, ~ 2 nm) placed in a glass beaker, also in free exchange with atmosphere (experiment DSM, Fig. 1A), *iii*) dialysis bags (6–8 kDa, ~ 2 nm) containing a solution of 10 mM NaHCO_3 and 10 mM of Mg were placed into a polycarbonate jar filled up with the same solution in which $1 \text{ g}_{\text{wet}} \text{ L}^{-1}$ of cyanobacteria *Synechococcus* sp. was added (experiment SD, Fig. 1B), *iv*) cyanobacterial suspension without BG-11 nutrient under light (experiment BSM), *v*) cyanobacterial suspension in the darkness (aerated bottles wrapped in aluminum foil; experiment CSM), and *vi*) abiotic experiments where NaOH was added to reproduce the increase of pH due to photosynthesis in biotic experiments (experiments AMg3, ASiMg3, ASiMg). All experiments were run at 25 ± 1 °C with an orbital shaker (for DSM) or under magnetic stirring (all other experiments) during 400 to 500 h. Biotic experiments were carried out under cool fluorescent lights of constant 2500 lx ($\sim 40 \mu\text{mol m}^{-2} \text{ s}^{-1}$, in duplicates and with abiotic controls. A 10% diluted BG-11 solution (freshwater cyanobacteria nutrient solution) was used as a nutrient source for bacteria except for BSM experiment. All manipulations were performed under sterile conditions in a laminar flow hood class A100. Note that, because the experimental solution was ca. 10 times enriched in DIC relative to the BG-11 culture media, there could not be limitation on cyanobacterial growth, even in the case of 90% DIC uptake in the course of experiment.

2.4. Sampling procedure

Samples were taken daily during the first week and then every 2–3

days in order to follow the evolution of different microbiologic and physicochemical parameters (biomass, pH, alkalinity, concentrations in Mg, Si and dissolved organic carbon (DOC)) and to characterize eventual precipitation of secondary minerals. An aliquot of 20 mL was taken during vigorous stirring to maintain the homogeneity of the suspension, and subdivided into several parts. The first 5 mL were used to measure the cyanobacterial concentration and the pH. The remaining 15 mL were centrifuged (3500 g, 30 min) and the supernatant was filtered ($0.45 \mu\text{m}$). A part of this filtrate was used to analyze the alkalinity (Alk), Si and DOC concentrations. The other part was acidified (2% HNO_3) to measure Mg^{2+} concentration. The filtrates were preserved at 4 °C pending analyzes.

2.5. Chemical analyzes

Cyanobacterial biomass was calculated from optical density of suspension at 680 nm ($\text{OD}_{680\text{nm}}$), using a Helios Epsilon spectrophotometer. The conversion factor from $\text{OD}_{680\text{nm}}$ to dry biomass ($\text{g}_{\text{dry}} \text{ L}^{-1}$) was equal to 0.519 and the ratio wet:dry biomass was 8 ± 0.5 . The pH was measured with a combination pH-electrode (Schott Geräte H62), with an uncertainty of 0.01 units. NIST buffers (pH = 4.00, 6.88, 9.22 at 25 °C) were used for the calibration of the electrode. The total silica concentration was measured by colorimetry with the molybdate blue method (Strickland, 1952) using a colorimetric chain Technicon Autoanalyzer II, with an uncertainty of 2% and a detection limit of $3 \times 10^{-7} \text{ M}$. Dissolved inorganic carbon (DIC) was calculated from pH and alkalinity, which was determined by a standard HCl titration using an automatic Schott TitroLine alpha plus titrator, with an uncertainty of 1% and a detection limit of $5 \times 10^{-5} \text{ M}$. Magnesium concentration was measured by flame atomic absorption spectroscopy in the oxygen-acetylene flame and 6 mA cathode source, using a Perkin Elmer AAnalyst 400 with an uncertainty of 1% and a detection limit of $1 \times 10^{-7} \text{ M}$. The DOC was determined using a Shimadzu TOC-V_{CSN} analyzer with an uncertainty of 5% and a detection limit of 0.1 $\text{mg C}_{\text{org}} \text{ L}^{-1}$.

The saturation indices were calculated using PHREEQC geochemical

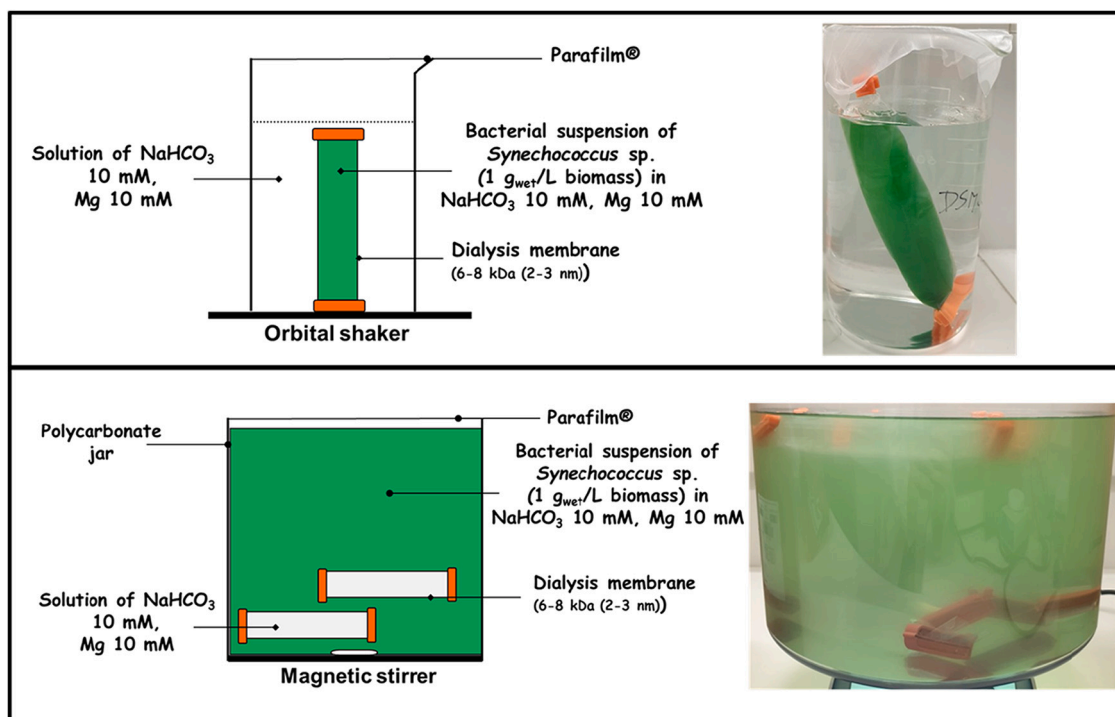


Fig. 1. Schematic representations and photos of experiments with cyanobacteria *Synechococcus* sp. inside (A, experiment DSM) or outside (B, experiment SD) of the dialysis bag.

code (Parkhurst and Appelo, 1999), with its *llnl.dat* database modified to consider new equilibrium constants in the Ca-Mg-CO₂-H₂O system from Palmer and Wesolowski (1997), Millero et al. (2007), Bénézeth et al. (2011), Stefánsson et al. (2013, 2014), Gautier et al. (2014), and Harrison et al. (2019).

Apparent rates of Mg, Si and DIC concentrations decrease (R_i , mmol L⁻¹ day⁻¹) were calculated for the stage of maximum precipitation, according to the following equations:

$$RMg = \frac{d[Mg]}{dt}, RSi = \frac{d[Si]}{dt}, RDIC = \frac{d[DIC]}{dt}$$

2.6. Microscopic analyzes

For SEM characterization, the aliquots of bacteria with precipitated mineral suspension were centrifuged (30 min, 1000 rpm) and the organic matter was removed from the solid phase by treating them in aqueous 10% H₂O₂ overnight. The remaining solids were rinsed three times with MilliQ water and freeze-dried at -50 °C. They were observed after carbon film coated on the sample surface with a JEOL JSM 6360LV SEM coupled with a SDD PGT Sahara EDS analyzer operating at 30 kV. The precipitated minerals and mineral-bacterial cell aggregates were also analyzed by X-ray diffraction using a D8-Advance Bruker diffractometer (Cu-Kα1 radiation, step size 0.0142 (2 θ), scan speed 10 s/step).

For TEM observations, first, the cell suspension was rinsed using sterile nutrient solution or MilliQ water and centrifuged 2 min at 7000 g. Samples were taken by immersing grids coated with a carbon film for 10 s in this MQ-rinsed bacterial suspension and dried several minutes to several hours at room temperature. It is possible that the drying procedure could lead to artefactual tight association of cells and minerals together and thus interfere with our interpretation of precipitation products. We tested the effect of the duration of the drying procedure on the resulting TEM images and did not detect any significant difference in cell and mineral size, shape and the degree of their association. Images of cell-free mineral suspension and mineral-free cell suspension yielded morphologies very similar to those in the ternary (cell+mineral in solution) systems. Another proof of the validity of the cell + carbonate mineral preparation procedure used in this study for planktonic cultures of cyanobacteria was acquired via confocal laser scanning microscopy (CLSM) as described in Bundeleva et al. (2014b).

Ultrathin slices for TEM examination were prepared from freshly sampled cells and precipitated minerals which were rinsed in MilliQ water, fixed with 2.5% glutaraldehyde/2% paraformaldehyde in 0.1 M Cacodylate buffer (pH 7.2) at ambient temperature for 1.5 h and then washed three times with 0.1 M Cacodylate, and subsequently soaked in 1% osmium tetroxide in 0.1 M Cacodylate buffer at ambient temperature for 1 h and finally washed three times with 0.1 M Cacodylate. The supernatant was removed and pellets were embedded in agarose, then samples were taken through stepwise ethanol dehydration (15 min at 25, 50, 70 and 90% ethanol at ambient temperature, and 3 × 30 min at 100% dry ethanol). Samples were then embedded in Epon EMBED 212 Resin and 80 nm thick ultrathin sections were processed with a Leica UCT ultramicrotome. Ultramicrocuts were mounted on Cu formvar-carbon grids, and post-stained with lead citrate. Then samples were characterized using TEM with a JEOL JEM-1400 HC (40–120 kV) and a JEOL JEM-2100F (200 kV, 2.3 Å resolution) equipped with a CMOS Gatan RIO16IS 4 K*4 K camera and coupled with a SDD Bruker EDS analyzer with an energy resolution of 127 eV.

3. Results

3.1. Aqueous solution evolution in the presence of cyanobacteria

Results of experiments with a monoculture of cyanobacteria *Synchococcus* sp. in a 10 mM NaHCO₃ solution with various Mg and Si concentrations are presented in Fig. 2A (10 mM Mg), 2B (10 mM Mg and 0.4 mM Si) and 2C (5 mM Mg and 0.3 mM Si). In experiments with 10

mM of Mg, the pH increased from 9 to 11.3 during the first 80 h, then it became stable until the end of experiments (Figs. 2A-B). Note that the pH and the concentration of DIC, Mg and Si were stable in blanks. The DIC was stable at 10 mM during the first 50 h then decreased by 90–95% during the next 150 h. The Mg concentration slightly decreased (~10%) during the first 50 h, and then further decreased two-folds during the following 100 h. In the experiment without Si, the Mg concentration remained stable until the end of the experiment (Fig. 2A), whereas it still decreased from 6 mM to 4 mM in the presence of Si (Fig. 2B). At 0.4 mM of initial Si, the Si concentration decreased by 99% during the first 150 h and then remained stable (Fig. 2B). The simultaneous sharp decrease of DIC, Mg and Si (when present) concentrations at high pH values suggested the precipitation of magnesium carbonates and/or silicates.

In experiments with 5 mM of Mg and 0.3 mM of Si, the evolution of different parameters was similar to the experiments previously described, with an increase of pH from 9 to 11.3 during the first 100 h, and a loss of 90% of DIC and 98% of Mg and Si between 100 and 240 h (Fig. 2C).

Considering the decrease of DIC, Mg and Si concentrations and the pH evolution in the course of experiments, the saturation indices (SI) calculated with PHREEQC indicated a possibility of precipitation of Mg carbonate and silicate minerals: artinite, hydromagnesite, dypingite, brucite and sepiolite (Figs. 2A-C). The SI values of artinite, brucite and hydromagnesite were negative at the beginning of experiments and increased to reach a maximum of 3, 2 and 5, respectively, between 70 and 100 h; subsequent decrease of SI indicated a possible formation of these minerals. The SI of nesquehonite was negative in all experiments. In experiments where Si was added (Figs. 2B-C), the SI of sepiolite was positive from the beginning until the end of experiments, and a decrease of Si after about 100 h of experiment indicated a possible precipitation of this mineral.

In experiments without 10% BG-11 nutrient medium (BSM), the pH increased from 8.5 to 9.6 between 0 and 96 h and remained stable until the end of the experiment (Fig. 3A). A lack of nutrients in the solution did not allow the cyanobacteria to metabolize and produce sufficiently high pH. Consequently, no precipitation was observed and the concentration of DIC remained stable at 10 mM. The Mg concentration decreased from 12 to 9.8 mM, which could be due to its uptake and adsorption by cyanobacteria for nutrient requirement.

During experiments in the darkness (CSM), cyanobacteria did not photosynthesize; thus, their biomass and solution pH remained stable. A decrease of Mg concentrations during the first 96 h may indicate a beginning of precipitation of Mg-bearing solid phases or Mg²⁺(aq) adsorption on cell surfaces (Fig. 3B). Increasing artificially the pH to 10 led to a decrease of DIC concentrations from 10 to 4 mM between 96 and 200 h. Further increase in pH to the value of 10.6 led to a rapid decrease of Mg concentration (from 9.8 to 7.2 mM in an hour). Thus, a concomitant decrease of both DIC and Mg concentrations indicated the formation of Mg carbonate in the solution.

During experiments with cyanobacteria which were confined within a dialysis bag (DSM), the photosynthetic activity induced an increase in pH inside and outside of the dialysis bags from 8.9 to 10 over the first 380 h of the experiment (Fig. 3C). Magnesium concentration slightly decreased from 13 to 11.5 mM during the first 24 h and then remained stable. The DIC concentration was stable at 10 mM during full duration of the experiment. Note that ion concentrations inside the dialysis bag were measured at the beginning and the end of the experiments and were similar to those outside of the bag (not shown). Even though pH increased, no precipitation was observed in these experiments.

When cyanobacteria were placed outside of the dialysis bag (SD), the pH value and Mg concentration were similar in and out of the bag, while the DIC was equilibrated between two compartments at 10 mM after 250 h of exposure (Fig. 3D). The pH increased from 8 to 11 in 400 h, the Mg concentration decreased from 12 to 8 mM between 0 and 300 h of experiment, and the DIC concentration decreased from 9.8 to 4 mM between 250 and 410 h of experiment, when pH reached a value of 10.5,

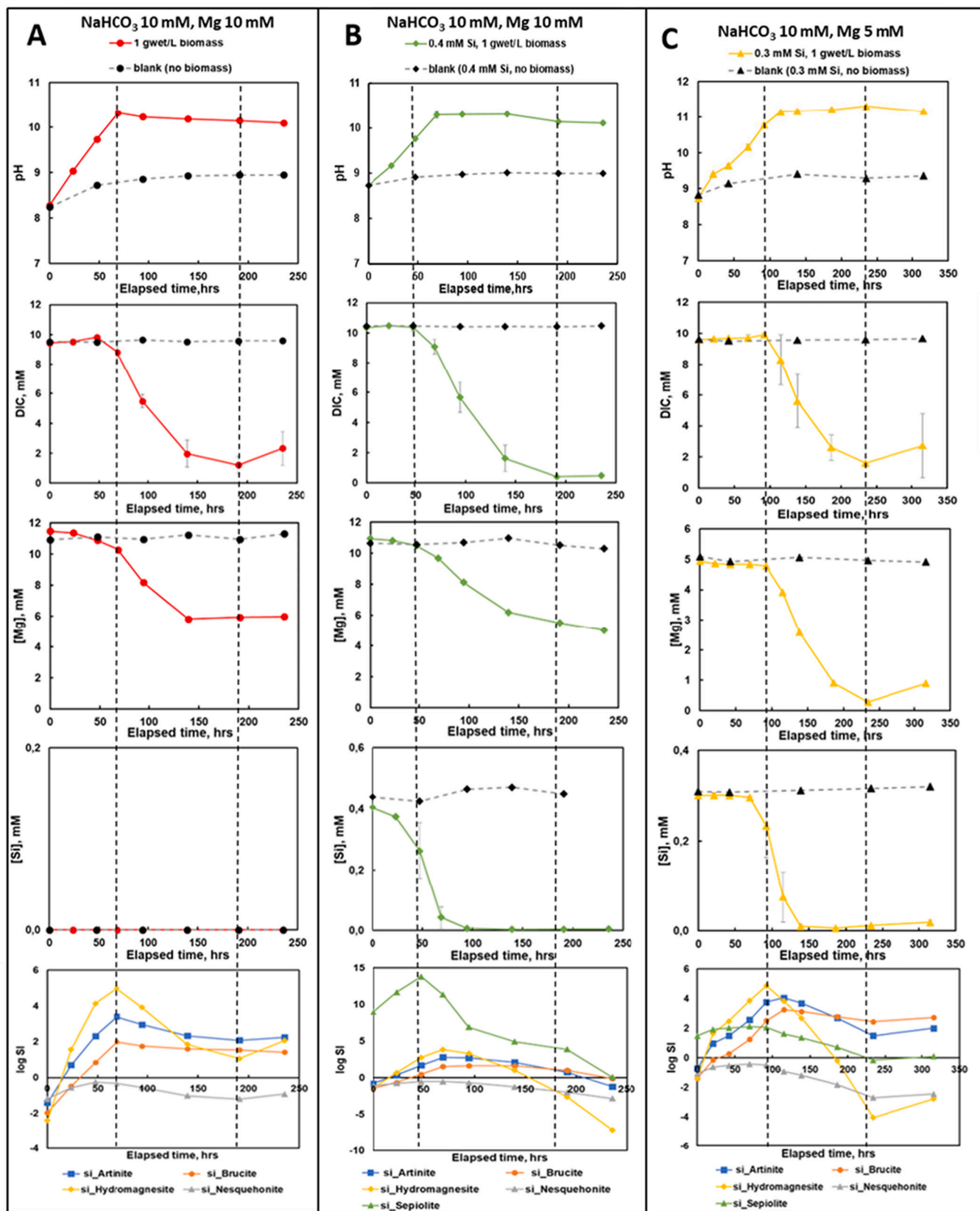


Fig. 2. Evolution of pH, concentrations in DIC, Mg and Si, and saturation indices (SI) of some carbonate or silicate magnesian minerals as a function of time in biotic experiments with cyanobacteria *Synechococcus* sp. and 10% BG-11 culture medium in a solution of NaHCO₃ 10 mM with A: 10 mM Mg, B: 10 mM Mg and 0.4 mM Si, C: 5 mM Mg and 0.3 mM Si. Error bars represent standard deviation of experimental replicates.

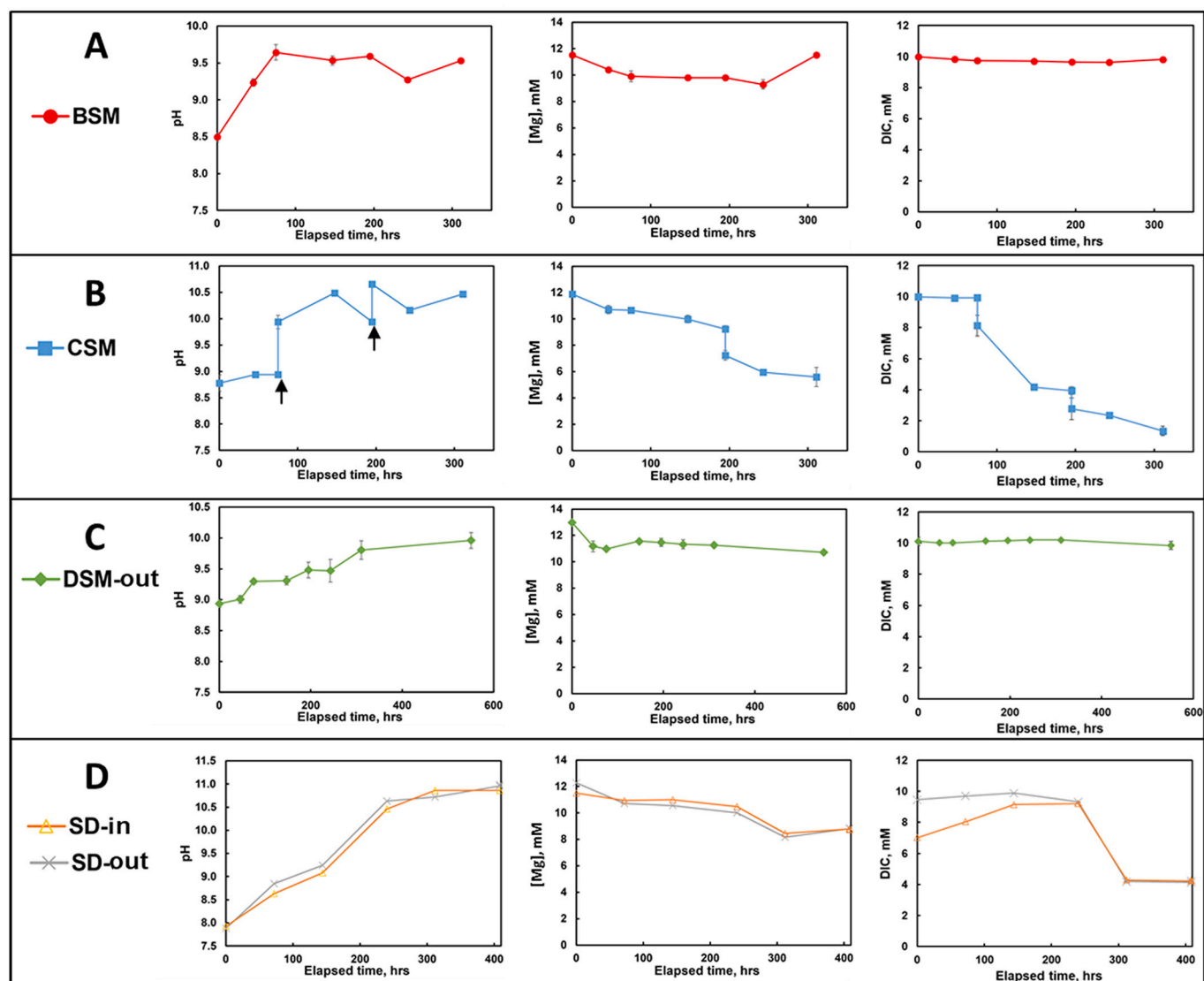


Fig. 3. Evolution of pH, Mg and DIC concentrations over time for biotic experiments without BG-11 culture media (BSM, A), in the darkness (CSM, B), with cyanobacteria inside the dialysis bag (DSM-out: sampling outside of the bag, C) and cyanobacteria placed outside of dialysis bag (SD-in and out: sampling respectively inside and outside of the bag, D). Error bars represent standard deviation of replicates.

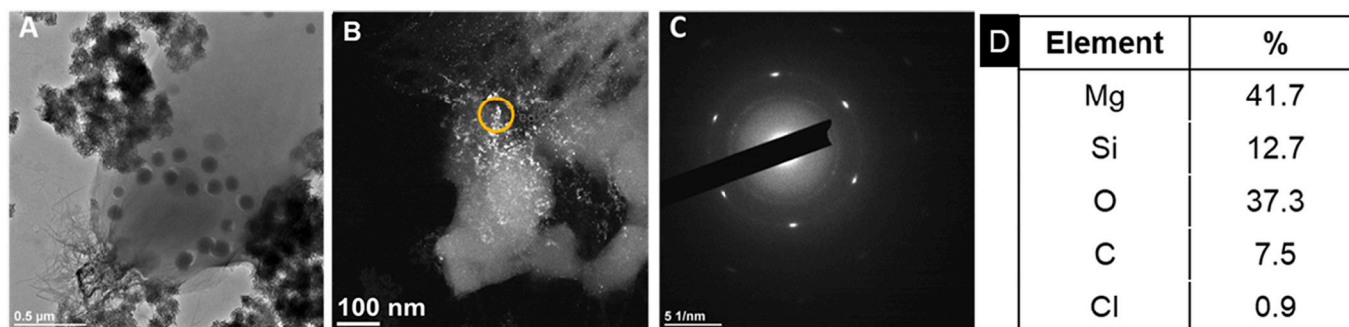


Fig. 4. TEM observations of the experimental cell suspension with formed minerals in the presence of 10 mM of NaHCO_3 with 10 mM of Mg and 0.4 mM of Si after one week of experiment. A: cell of *Synechococcus* sp. in the center, presence of a solid fibrous phase near the cell (at the top and bottom right of the picture), and needles in the vicinity of the bacteria, B: picture in dark field to highlight the nanocrystals (white dots on the picture), C: SAED realized in the orange circle in panel B, D: composition of the particles in the orange circle according to the EDS analysis. Multiple EDS analyses ($n = 7$ to 10) were performed at various spots of nanocrystals association.

thus indicating the precipitation of Mg carbonate. The formation of this phase was clearly observed outside the dialysis bag in the form of a mixture of the mineral deposit and cyanobacterial biomass at the bottom of the reactor and on its walls (Fig. S1A), as well as on the external surface of the dialysis bags (Figs. S1B–C).

3.2. Microscopic and spectroscopic characterization of solid phases formed during the biotic experiments

In order to reveal the relationship between cyanobacterial cells and precipitated mineral phase(s), the experimental suspension was examined with transmission electronic microscopy (TEM) after one and two weeks of experiment with 10 mM of Mg and 0.4 mM of Si in the initial solution (Figs. 4 and 5). After first week, a solid fibrous phase was visible around the cyanobacteria cells (Fig. 4A, top and bottom right). Thin, hair-like needles were detectable in the immediate vicinity of the cell (shown at the bottom of Fig. 4A). The observation in dark field using a diaphragm allowed to distinguish the crystalline particles, appearing in bright white on Fig. 4B, from the amorphous phase appearing in grey on the same figure. The Selected Area Electron Diffraction (SAED) pattern confirmed the presence of a crystalline phase (Fig. 4C) particularly in the zone encircled in red on Fig. 4B, where the quantity of particles was the highest. After two weeks of experiments, cyanobacteria were surrounded by some solid phase (Fig. 5A). Near the cells, nanometric white particles were clearly detectable (encircled in the left, Fig. 5B). At some distance from the cells (100–200 nm), thin needles were present (Fig. 5B, in the right circle). At the same time, at the end of experiment, solid fibrous phase was not detectable anymore. The SAED pattern indicated the presence of a crystalline phase in the spots where the largest amount of nanoparticles was concentrated (Fig. 5C). An energy dispersive X-ray spectrometry (EDS) analysis allowed the determination of the chemical composition of the crystalline phases after one and two weeks of experiment (Figs. 4D and 5D, respectively). After subtracting of background from the carbon film signal, these phases contained mostly magnesium (~ 40%), oxygen (~ 35%) and carbon (7 to 17%). Hence the crystallized phases could be hydrous magnesian carbonates. In the sample retrieved after one week of reaction, silicon was also present (12%), which could correspond to a magnesian silicate such as sepiolite. No crystalline phase was detected within the needles. However, the needles could be too thin (i.e., less than 10 nm wide) to reveal the nature of constituent minerals.

The TEM observations of the experimental suspension collected outside the dialysis bags (experiment SD) revealed a crystalline phase near the *Synechococcus* cells (Figs. 6A–B). According to the EDS analysis realized in the red circle on Fig. 6B, this phase contained mostly carbon (47%), magnesium (38%) and oxygen (13%) (Fig. 6D), which could indicate the presence of hydrous Mg carbonate. In the sample collected from the experiment in the darkness (CSM), a crystallized precipitated phase composed of Mg, C and O was also present but no cells were

visible, and there was only some residual organic matter from the bacterial cells which were present at the beginning of the experiment (Fig. S2).

The SAED patterns obtained from the crystalline phases after one and two weeks of experiments (Figs. 4C and 5C, respectively) and from the experiment SD in the dialysis bag (Fig. 6C) yielded an average lattice thickness of 0.153 nm, which is similar to the major reflection of either nesquehonite ($\text{MgCO}_3 \cdot 3\text{H}_2\text{O}$; d_{101} , 100% intensity) or hydromagnesite ($\text{Mg}_5(\text{CO}_3)_4(\text{OH})_2 \cdot 4\text{H}_2\text{O}$; d_{110} , 73% intensity). However, due to overall weak signal, we could not distinguish between two minerals. Thus, further in-depth XRD analyses or mineral structures information from the SE-SEM performed on large amount of mineral phase precipitated in specially designed experiments would be necessary to reveal the exact identity of hydrous Mg carbonates.

In order to observe the fine features of mineral precipitation in the vicinity of the cells, a cross-sectional TEM observation of organo-mineral aggregates formed in SiMg3 experiment during 2 weeks of incubation was also realized (Fig. 7). A longitudinal section of the cyanobacteria *Synechococcus* sp. (Fig. 7 A, B) revealed a black photosynthetic membrane and dark spherical formations corresponding to intracellular phosphate globules or Ca oxalate crystals consistent with previous observations (Lamérand et al., 2020). Some mineral solid phase was also present outside the cells (Fig. 7 C, D black formations). Finally, some filaments were visible on the cell membrane (Fig. 7 C, D); however, they were too thin to be characterized by EDS analysis. These could be EPS released by the bacteria during their metabolic activity.

3.3. Abiotic experiments

In abiotic experiments, we artificially increased the pH via progressive addition of NaOH to approximate a temporal pattern of the pH rise due to photosynthesis in the biotic experiments. The precipitation of hydrous Mg-carbonate and Mg-silicate occurred when the pH reached the value of ~10.3, accompanied by a simultaneous decrease of DIC, Mg and Si (when present) concentrations in solution (Figs. S3 A–C).

SEM observations of the mineral formed during the experiment showed the presence of rosette-like crystals in the experiment AMg3 (Figs. 8A–B), similar to Mg carbonate hydromagnesite and dypingite as demonstrated in our previous study with the same cyanobacteria (Lamérand et al., 2020). These crystals were partially visible in the experiment ASiMg3 (Figs. 8C–D) together with a granular, probably amorphous phase, which was the only one visible in the ASiMg experiment (Figs. 8E–F). These observations were confirmed by XRD analysis, which showed a mixture of hydromagnesite and dypingite in the sample from AMg3 experiment, whereas no crystalline phase was detected in the samples from Si-bearing abiotic experiments (ASiMg3 and ASiMg) as illustrated in Fig. S4 of the Supplement.

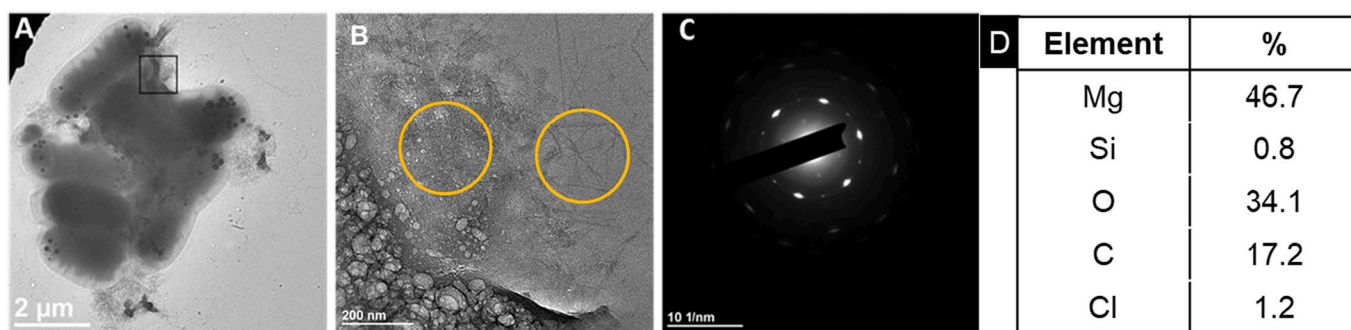


Fig. 5. TEM observations of the experimental cell suspension with formed minerals in the presence of 10 mM of NaHCO_3 with 10 mM of Mg and 0.4 mM of Si after two weeks of experiments. A: group of cyanobacteria *Synechococcus* sp., B: zoom on the part framed in black on A, C: SAED realized on the part encircled in orange on the left on panel B, D: composition of the particles in two orange circles (B) according to multiple ($n = 7$ to 10) EDS analysis.

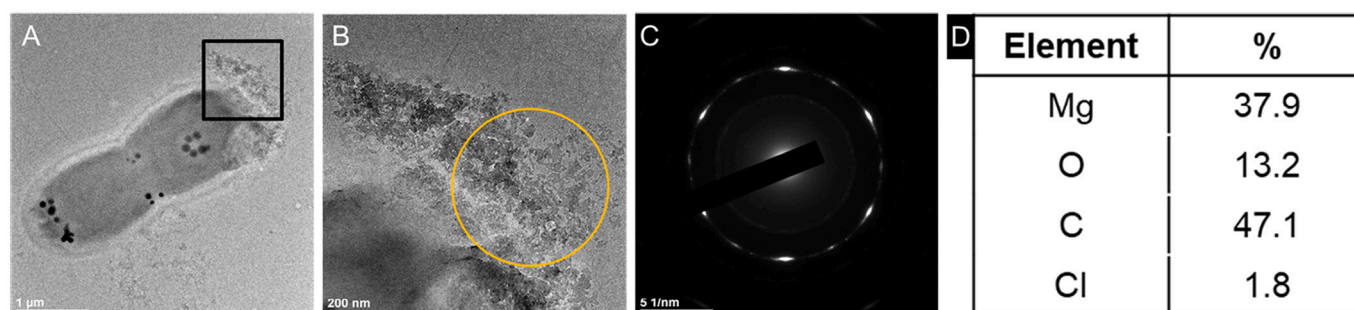


Fig. 6. TEM observations of bacterial cells collected outside the dialysis bags in the experiment SD. A: cyanobacteria *Synechococcus* sp., B: zoom on the part framed in black on A, C: SAED realized on the part circled in orange on B, D: composition of the particles in the orange circle according to the EDS analysis.

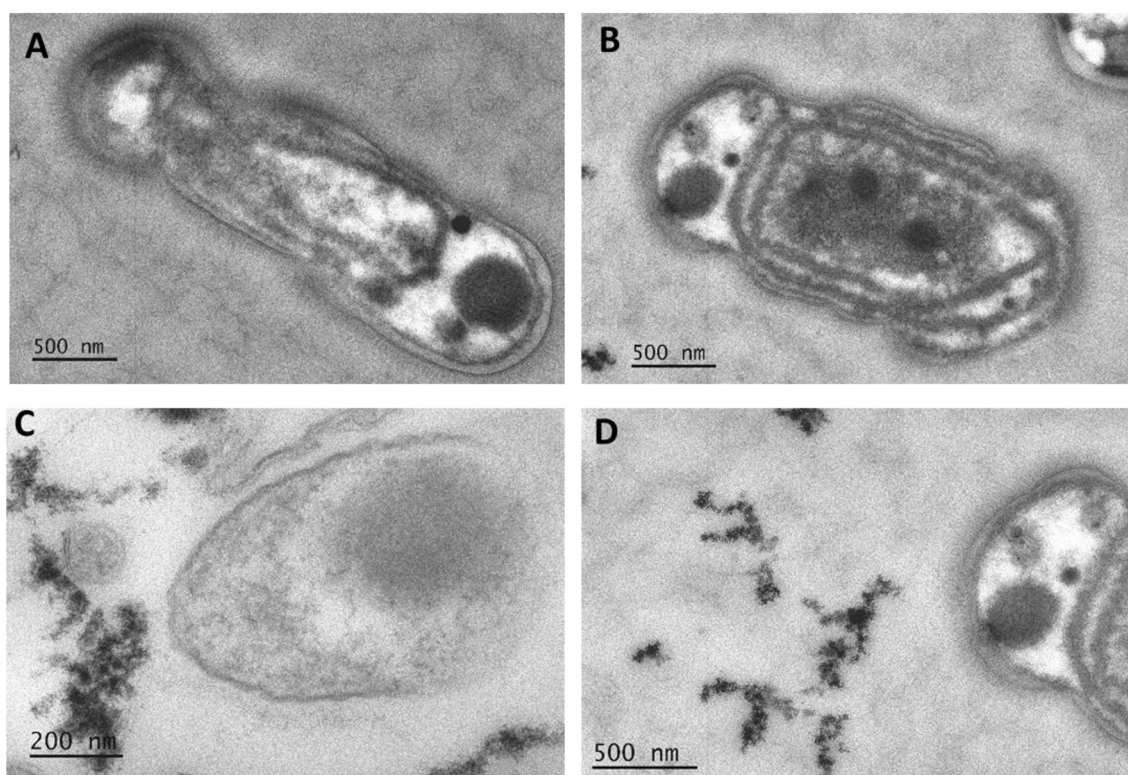


Fig. 7. TEM cross-sections of *Synechococcus* sp. in a solution of 10 mM of NaHCO_3 enriched with 10 mM of Mg and 0.4 mM of Si. A, B: longitudinal section of *Synechococcus* sp., C, D: cross section of *Synechococcus* sp., showing solid particles on the left, cell of *Synechococcus* sp. on the right.

3.4. Rates of precipitation

Apparent rates of Mg, Si and SIC concentration decrease are listed in Table 2. In most experiments, a higher initial Mg concentration led to a faster decrease of Mg and DIC concentrations. Under the same initial conditions, the rate of DIC decrease was similar for abiotic and biotic experiments. In the abiotic experiments, a decrease of Mg concentration was slightly slower ($0.62\text{--}0.96\text{ mmol L}^{-1}\text{ day}^{-1}$ compared to $0.76\text{--}1.5\text{ mmol L}^{-1}\text{ day}^{-1}$ in the biotic experiments). This difference could be explained by intracellular consumption and/or surface adsorption of Mg by cyanobacteria in biotic experiments in addition of Mg precipitation, while in the abiotic experiments, only the precipitation occurred. The magnitude of Si concentration decrease was similar regardless the initial Si concentration but the apparent rate was faster in abiotic experiments compared to biotic experiments ($\sim 0.2\text{ mmol L}^{-1}\text{ day}^{-1}$ and $\sim 0.1\text{ mmol L}^{-1}\text{ day}^{-1}$, respectively).

4. Discussion

4.1. Precipitation of secondary minerals: Rates and identity of secondary phases

Distinct precipitation of secondary minerals was observed in a biotic carbonate-bearing environment with different concentrations in Mg and Si. Fast and simultaneous decrease of the Mg and Si (when present) concentrations in biotic experiments ($1\text{ g}_{\text{wet}}\text{ L}^{-1}$ of biomass, Fig. 2) indicated the precipitation of magnesian carbonates and/or silicates, highlighting the governing role of cyanobacteria in the secondary phase formation. Indeed, during the photosynthesis, cyanobacteria increased the pH above 10.3 (Fig. 2), thus rising significantly the supersaturation degree of solution with respect to artinite, hydromagnesite, brucite and sepiolite. This induced the precipitation of Mg-bearing phases which could not be formed at lower pH values.

The observation by TEM coupled with EDS analysis highlighted the presence of crystalline hydrous Mg carbonate phases in the vicinity of

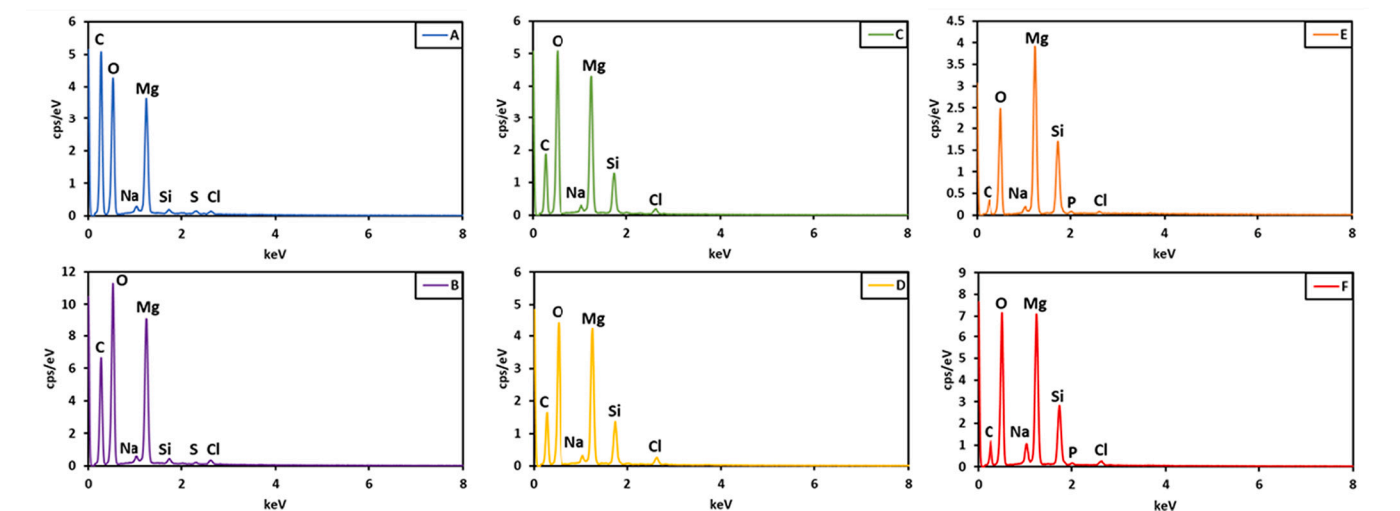
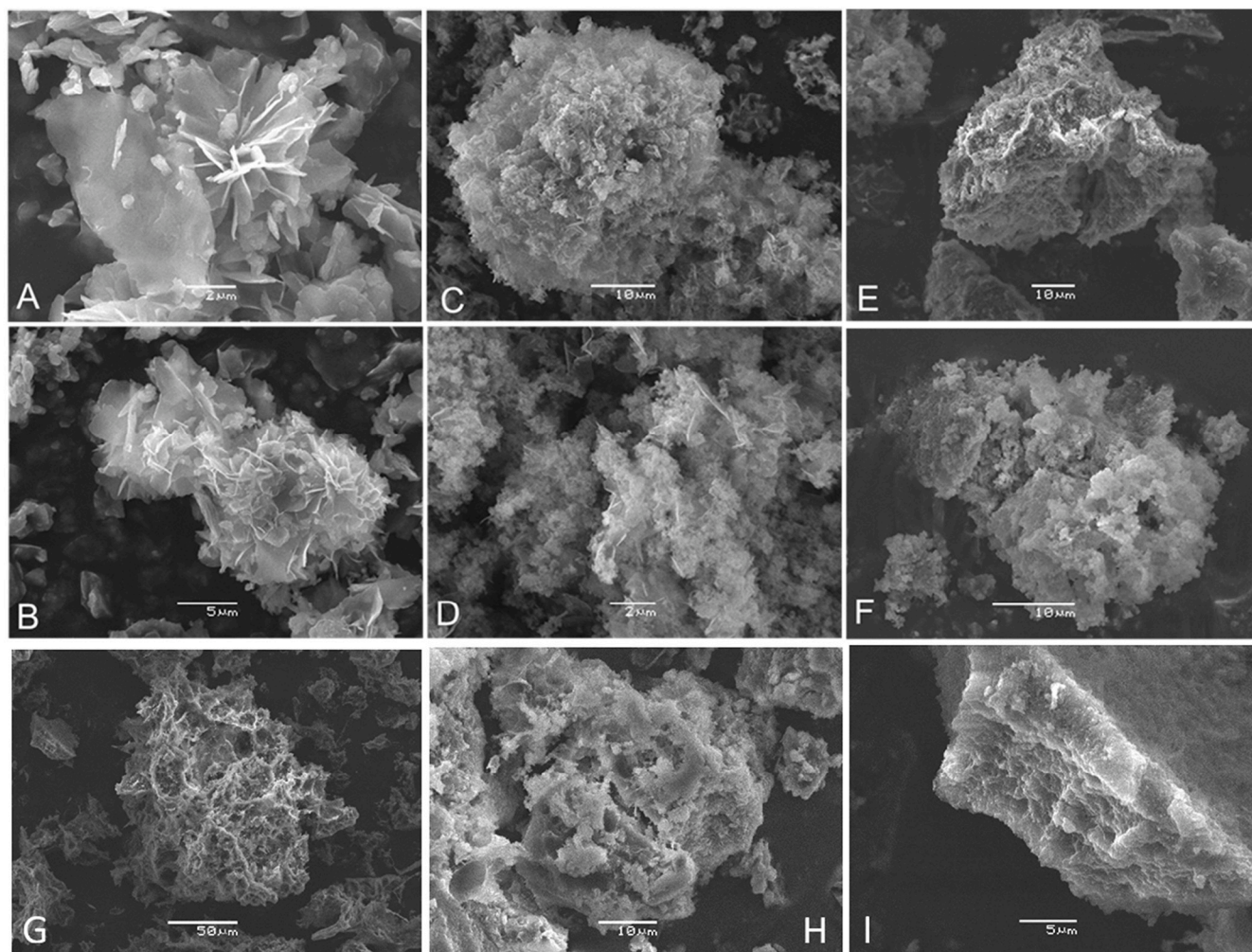


Fig. 8. SEM pictures of the precipitated phases from abiotic experiments AMg3 (A and B), ASiMg3 (C and D), ASiMg (E and F) and biotic experiments SiMg (G, H) and SiMg3 (I) after 1 week of cell culture. Experimental conditions are listed in Table 1. The main elements detected by EDS point analyses are Mg, O, C (panel A and B) and Mg, O, C and Si (panel C to I).

bacterial cells (Figs. 4-7). The SAED patterns allowed identifying these minerals as nesquehonite and/or hydromagnesite, whereas temporal evolution of saturation indices during experiments indicated the possible precipitation of hydromagnesite but not nesquehonite. However, at the surface of cells, in the cell phycosphere, the pH is sizably

higher than that measured in the bulk solution (Revsbech et al., 1983; Dupraz et al., 2009). Although this is generally applied to cyanobacterial biofilms, unicellular photosynthesizing plankton is also likely to exhibit a pH gradient suitable for precipitation of carbonate minerals (Pokrovsky and Savenko, 1995). Therefore, cyanobacterial photosynthesis could

Table 2

Variations of concentrations of DIC, Mg and Si and rates of Mg, Si and DIC concentrations decrease (respectively R_{Mg} , R_{Si} and R_{DIC} , $\text{mmol L}^{-1} \text{day}^{-1}$) during the stage of maximal concentration change (solid phase precipitation). Dash sign means that there was no measurable change in concentration and thus the rate could not be calculated.

	ΔDIC , mM	$\Delta[\text{Mg}]$, mM	$\Delta[\text{Si}]$, mM	$\Delta\text{DIC}/\Delta[\text{Mg}]$	$\Delta[\text{Mg}]/\Delta[\text{Si}]$	R_{Mg}	R_{Si}	R_{DIC}
SiMg	8.32	4.51	0.29	1.85	15.6	0.76	0.10	1.41
Mg3	7.50	4.91	–	1.53	–	1.51	–	2.33
SiMg3	9.88	5.49	0.26	1.80	21.1	1.19	0.12	1.66
ASiMg	5.82	2.54	0.44	2.29	5.77	0.62	0.21	1.40
AMg3	4.83	1.81	–	2.67	–	0.69	–	2.09
ASiMg3	5.67	1.70	0.58	3.34	2.93	0.96	0.27	1.40
BSM	–	–	–	–	–	–	–	–
CSM	8.64	6.31	–	1.37	–	1.64	–	1.43
DSM	–	–	–	–	–	–	–	–
SD	5.13	4.11	–	1.25	–	0.61	–	1.28

have induced a much higher local supersaturations leading to the crystallization of nesquehonite. The nesquehonite is the first phase to precipitate in the Mg-CO₂-H₂O system at 25 °C, in the presence or absence of cyanobacteria (Mavromatis et al., 2012; Hopkinson et al., 2012; Shirokova et al., 2013). This freshly precipitated phase could have evolved over time into hydromagnesite as it is known from other biotic and abiotic experiments (Mavromatis et al., 2012; Harrison et al., 2021).

Variations of DIC, Si and Mg concentrations were calculated between the beginning and the end of the main precipitation stage (Table 2). This allowed assessing the ratios of DIC to Mg concentrations in the solid phase which ranged between 1.25 and 3.34. These values are higher than those of hydromagnesite (0.8) and nesquehonite (1), and consistent with a mixture of different magnesian carbonate phases. The apparent Mg rates during the fastest precipitation stage in both abiotic and biotic experiments varied between 0.61 and 1.64 $\text{mmol Mg L}^{-1} \text{day}^{-1}$. They are of the same order of magnitude than those calculated from the data of Shirokova et al. (2013) in Si-free solutions which varied from 0.31 to 2.88 $\text{mmol Mg L}^{-1} \text{day}^{-1}$.

In biotic experiments where the formation of Mg carbonate was observed, the ratio of Mg decrease to organic carbon produced ($\Delta\text{Mg}/\Delta\text{C}_{\text{org}}$) during the course of experiment was calculated considering that the proportion of carbon in dry biomass is 50%. This ratio was equal to 0.24, 0.45, 0.37, 0.22 and 0.73 for the experiments SiMg, Mg3, SiMg3, DSM and SD, respectively (see Table 1 for abbreviation of experimental conditions). These values are inferior to the theoretical Mg/C_{org} ratio of 1 for nesquehonite as first precipitating phase during cyanobacterial photosynthesis:



Therefore, one can assume that the efficiency of cyanobacterially-induced precipitation of hydrous Mg carbonate is partially decreased due to the presence of aqueous Si, and a part of Mg resides within amorphous Si–Mg compounds.

4.2. Mechanisms of biomineralization and the role of sepiolite as a precursor of carbonate mineral formation

A solid fibrous phase observed via TEM in the biotic experiment containing 10 mM of Mg and 0.4 mM of Si did not show any crystalline order; however these formations strongly resembled to sepiolite recently synthesized in laboratory (Baldermann et al., 2018) (Fig. S5). The latter study was performed under abiotic conditions at different Si:Mg ratios, and reported the precipitation of sepiolite after 2 to 3 months. One of their experiments (Si:Mg = 1:28) corresponded to Si:Mg ratio in our experiment (10 mM Mg and 0.4 mM Si). In our case, no abiotic precipitation of sepiolite was observed; presumably, the relatively short duration of the experiments (two weeks) was not sufficient to allow the abiotic formation of this mineral. However, in biotic experiments, the bacterial metabolism and the associated increase of pH could have induced the precipitation of sepiolite, via increasing the saturation index

of this mineral (Fig. 2). This is a notable result which demonstrates a strong power of bacteria to accelerate the precipitation of minerals whose abiotic formation is thermodynamically possible but delayed because of the low rate and the kinetic barriers of nucleation. Presumably, cyanobacterial cells and their exopolysaccharides can act as mineral nucleation centers by decreasing activation energies (Dupraz et al., 2009) thus rendering possible the precipitation of sepiolite already after the first week of incubation.

Another interesting result of this study is that the sepiolite can serve as a precursor of hydrous Mg carbonate formation. According to multiple EDS analyses ($n = 7$ to 10 spots) of the biotic experiment reaction products illustrated in (Figs. 4D, 5D), the sepiolite (or sepiolite-like amorphous material) decreased its relative abundance between 1 and 2 weeks of incubation as reflected in a ten-fold decrease of Si concentration in the solid phase and disappearance of needle-like solid phase in the TEM images (Fig. 4 A, 5 A). This observation is consistent with a hypothesis of hydrous Mg silicate providing Mg for in-situ hydrous Mg carbonate precipitation via coupled dissolution/precipitation reaction. Such an explanation was recently put forward by Pace et al. (2016) to explain in-situ dolomite/protodolomite formation in the vicinity of natural biofilm producing both Mg, Ca carbonate, protodolomite and sepiolite.

The dark spheric formations observed inside the cells of cyanobacteria (Fig. 7) were similar to amorphous calcium carbonates intracellularly precipitated by several cyanobacteria, such as *Synechococcus* sp. PCC 6312 or *Synechococcus* sp. PCC 6716 (Benzerara et al., 2014). However, according to a former study of the precipitation of secondary minerals in presence of *Synechococcus* sp. PCC 7942, these were phosphate globules, initially present in the cells before the beginning of the experiments (Lamérand et al., 2020).

In abiotic experiments, the increase of pH via the addition of NaOH led to the precipitation of hydrous Mg carbonates, thus indicating that the main driving factor of biomineralization is the photosynthetically-induced pH increase. However, production of alkaline environment is not always sufficient for extracellular Mg silicate and carbonate formation. Indeed, separating the cyanobacteria from the bulk of aqueous solution via enclosing them in the dialysis bag (< 2–3 nm pore size) yielded the precipitation solely inside the dialysis compartment (Fig. S1), despite of identical chemical composition of aqueous solution (pH, Mg, DIC, saturation state) inside and outside the dialysis compartment at the end of experiment. This strongly suggests that cyanobacterial cells and their EPS which were retained by dialysis membrane, serve as nucleation centers to promote the mineralization. As such, the limiting step of bio-carbonation could be the presence of bacterial cells whose surfaces provided a template for nucleation. Another explanation could be that Mg-carbonate / Mg-silicate nucleation clusters that were formed in the microenvironment around the cells inside the dialysis bag were too large to pass through the pores of the dialysis membrane, and thus the majority of precipitation occurred in the vicinity of bacterial suspension. It is thus possible that local rise of

pH in the cell phycosphere at the very beginning of dialysis experiment led to immediate removal of Mg in the form of hydrous Mg carbonates or silicates micro-clusters, having the size >3.5 kDa. This depleted the external solution and prevented it reaching necessary threshold of S.I. for spontaneous mineral precipitation. This mechanism can explain an apparent contradiction between results of abiotic and dialysis experiments. In this regard, temporal evolution of aqueous solution composition inside and outside the dialysis bag would allow better resolving the early stages of mineral formation in the presence of cyanobacteria.

The processes of precipitation of magnesian carbonates by cyanobacteria could be similar to those of calcium carbonates. The latter are well studied in various phototrophic bacterial systems (Aloisi, 2008; Bundeleva et al., 2014b; Cam et al., 2018; Dittrich et al., 2003, 2004; Lee et al., 2006). Following this path, we suggest that, first, Mg^{2+} ions accumulate at the surface of the cells because of electrostatic interactions between the negatively charged groups of the cells surface (carboxylates, hydroxylates, phosphorylates) and the Mg^{2+} cations (Douglas and Beveridge, 1998). This is further stimulated by the presence of EPS which could act as nucleation centers (Dittrich and Obst, 2004), via decreasing the interfacial energy and providing sizeable amount of cation-binding moieties (Priester et al., 2006; Guibaud et al., 2008; Kantar et al., 2011). Aqueous carbonate and bicarbonate anions may interact with these cations to form carbonate minerals, near the cells and in their capsules (Miller et al., 1990). Another possible mechanism, suggested for the first time by Douglas and Beveridge (1998) for *Synechococcus* cells suspended in Fayetteville Green Lake water and producing massive gypsum or calcite deposits is the continuous release of mineralized S-layer by the cells, quickly replaced by new polymeric molecules. This may produce biominerals located at some distances from the cell surfaces, as also seen in our TEM images. Such a pathway does not require any specific protection mechanism against cell encrustation by newly formed minerals, unlike the one which operates for $CaCO_3$ - *Synechococcus* sp. system (Martinez et al., 2010; Bundeleva et al., 2014b).

To resume, macroscopic experiments, thermodynamic calculations and TEM observations suggest the following mechanism. First, an amorphous magnesium silicate and nanocrystals of Mg carbonates are

formed around the cells, then these precursors are dissolved, liberating Mg in the fluid. Nanocrystals of nesquehonite are formed in the vicinity of the cells, and they gradually assemble themselves into thin needles. Over time, a part of these crystals could transform into more stable magnesium carbonate such as hydromagnesite or dypingite, as it is known from abiotic experiments (i.e., Harrison et al., 2021).

4.3. CO_2 sequestration capacity via hydrous Mg carbonate biomineralization by cyanobacteria

During the CO_2 biomineralization by cyanobacteria, carbon can be sequestered (i.e., removed from solution) via two pathways: as organic carbon (C_{org}) during the production of biomass (both the biomass and soluble exometabolites), and as inorganic carbon (C_{inorg}) during the formation of carbonate minerals. There is also a possibility of CO_2 release as the carbonate system compensates for the change of alkalinity, despite the fact that the majority of mineral precipitation in this study occurred at pH 10...10.5 when at least half of DIC is present in the form of CO_3^{2-} (aq). Furthermore, net CO_2 sequestration requires a presence of primary minerals that supplies cations such as the case of olivine dissolution in the presence of cyanobacteria (Bundeleva et al., 2014a) or microbial consortia (Lamérand et al., 2020). In this study we focused on rates and mechanisms of more general case of C sequestration both as microbial biomass and secondary minerals. The quantity of sequestered C_{inorg} was estimated via mass-balance calculation from a decrease of DIC concentration between the beginning and the end of the experiment. The amount of C_{org} formed in the experiment is composed of particulate organic carbon (POC) which corresponds to half of the dry biomass, and DOC in the form of exometabolites and EPS. Carbon sequestration potential (CSP) was calculated via dividing the quantity of sequestered carbon by the time it took to be sequestered. We estimated that carbon was mostly (ca 60–70%) sequestered in particulate organic form (Fig. 9). Soluble exometabolites and EPS (DOC) contributed to only 2–10% of the total CSP. The quantity of C sequestered in the mineral form (from DIC) was similar in biotic and abiotic experiments (0.7 – 1.2 $mmol L^{-1} day^{-1}$). The presence of Si in the solution slightly increased ($\sim 20\%$) the quantity of sequestered inorganic carbon, whereas there was no correlation

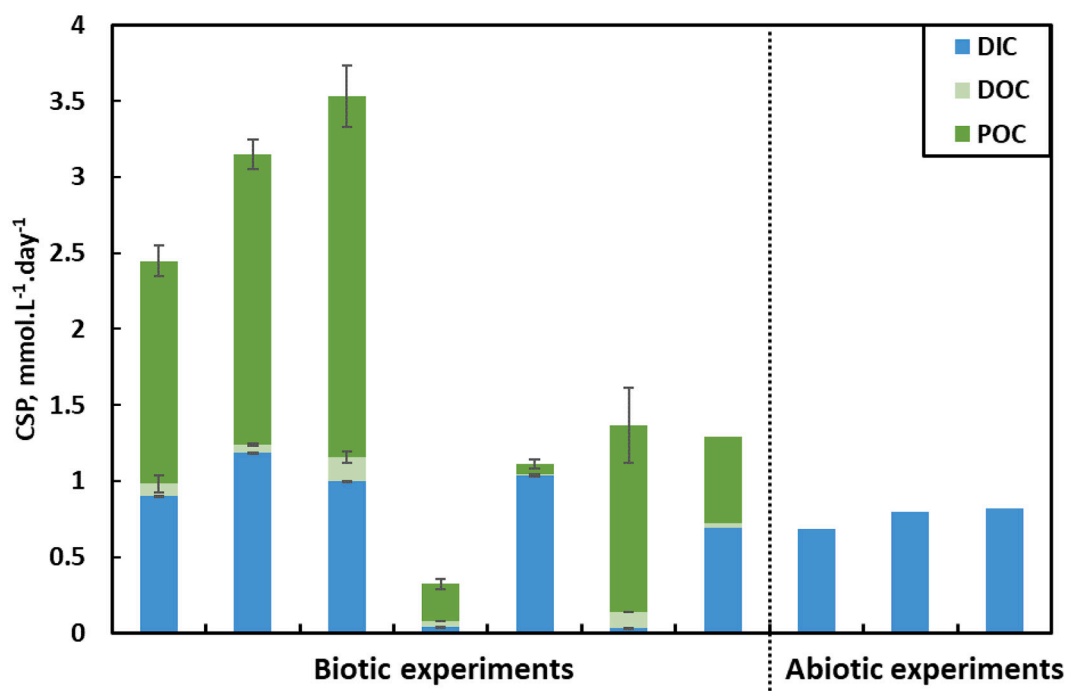


Fig. 9. Comparison of carbon sequestration potential in biotic and abiotic experiments. Error bars represent standard deviation of replicates. Three forms of CO_2 sequestration – DIC, DOC and POC – represent mineral, soluble organic matter and cell biomass. See Table 1 for experimental conditions.

between the quantity of aqueous Mg in the initial solution and the CSP. Overall, biotic experiments with nutritive medium and without dialysis bags (Mg3, SiMg3 and SiMg) exhibited the highest carbon sequestration potential because of the large quantity of C sequestered in the biomass during the development of cyanobacteria. This shows the potential of cyanobacteria to sequester carbon, by both the biomass they produce and the carbonate minerals they stimulate to precipitate in highly alkaline environment.

5. Conclusions

The biomineralization of carbon dioxide is an important process to consider in CO₂ storage and sequestration techniques. During this study, the role of cyanobacteria in the precipitation of carbonate phases was examined at variable biological and physicochemical parameters (cyanobacterial biomass, pH, Mg, Si, DIC, DOC concentrations) over 10 to 14 days of reaction. The rates of Mg carbonate precipitation were comparable to those observed in previous experiments with Si-free aquatic systems of Mg carbonates and cyanobacteria and were unaffected by Mg:Si ratio in the initial solution.

Obtained results demonstrate strong control of the cyanobacterial activity on hydrous carbonate (nesquehonite and hydromagnesite) and Mg silicate mineral precipitation. The dominant mechanisms include the increase in pH near the cells during the photosynthesis and the release of exopolymers that can serve as nucleation centers and thus trigger carbonates and silicates precipitation from supersaturation solution. The dialysis experiments demonstrated incontestable role of cyanobacterial surfaces, serving as templates for both Mg silicate and carbonate precipitation. The TEM observations highlighted the formation of crystalline magnesian carbonated phases in the vicinity of cells. The minerals formed could be a mixture of nesquehonite and hydromagnesite. A magnesium silicate such as sepiolite or its poorly crystalline analogue could also be present at the beginning of biomineralization reaction. This suggests its possible role as a precursor of carbonate minerals, which is consistent with recent natural observations. The overall C sequestration in the organic and mineral form was dominated by particulate organic C (in the form of bacterial biomass) with ca. 35% of C sequestered in the form of hydrous Mg carbonates.

Declaration of Competing Interest

The authors declare no Competing Interest.

Acknowledgements

Supports from grants BIOCASTRO of MITI (CNRS), SERPCARB (Carnot ISIFoR), BIOMIN (Interrvie INSU-CNRS) and CaBioCa of Défi (Action conjointe, MITI CNRS) are acknowledged. OP acknowledges support from the Tomsk State University Development Program “Priority-2030”.

Appendix A. Supplementary data

Supplementary data to this article can be found online at <https://doi.org/10.1016/j.chemgeo.2022.120854>.

References

- Aloisi, G., 2008. The calcium carbonate saturation state in cyanobacterial mats throughout Earth's history. *Geochim. Cosmochim. Acta* 72, 6037–6060.
- Balan, E., Noireaux, J., Mavromatis, V., Saldi, G., Montouillout, V., Blanchard, M., Pietrucci, F., Gervais, C., Rustad, J.R., Schott, J., Gaillardet, J., 2018. Theoretical isotopic fractionation between structural boron in carbonates and aqueous boric acid and borate ion. *Geochim. Cosmochim. Acta* 222, 117–129.
- Baldermann, A., Mavromatis, V., Frick, P.M., Dietzel, M., 2018. Effect of aqueous Si/Mg ratio and pH on the nucleation and growth of sepiolite at 25°C. *Geochim. Cosmochim. Acta* 227, 211–226.
- Barbiero, L., Queiroz Neto, J.P., Ciornei, G., Sakamoto, A.Y., Capellari, B., Fernandes, E., Valles, V., 2002. Geochemistry of water and ground water in the Nhecolândia, Pantanal of Mato Grosso, Brazil: variability and associated processes. *Wetlands* 22, 528–540.
- Barbiero, L., Rezende Filho, A., Furquim, S.A.C., Furian, S., Sakamoto, A.Y., Valles, V., Graham, R.C., Fort, M., Ferreira, R.P.D., Queiroz Neto, J.P., 2008. Soil morphological control on saline and freshwater lake hydrogeochemistry in the Pantanal of Nhecolândia, Brazil. *Geoderma* 148, 91–106.
- Bénéth, P., Saldi, G., Dandurand, J.L., Schott, J., 2011. Experimental determination of the solubility product of magnesite at 50 to 200°C. *Chem. Geol.* 286, 21–31.
- Bénéth, P., Godard, M., Thion, I.P., Gouze, P., Wolff-Boenisch, D., Laurent, L., Cluzel, D., Audigane, P., Monnin, C., Augé, T., Ménez, B., Baby, P., Kelemen, P., 2014. Report of the project Stockage Géologique du CO₂ in situ en Nouvelle-Calédonie. CNRT Nickel et Environnement. (83 pp).
- Benzerara, K., Skouri-Panet, F., Li, J., Féraud, C., Gugger, M., Laurent, T., Couradeau, E., Ragon, M., Cosmidis, J., Menguy, N., Margaret-Oliver, I., Tavera, R., López-García, P., Moreira, D., 2014. Intracellular Ca-carbonate biomineralization is widespread in cyanobacteria. *P. Natl. Acad. Sci. USA* 111, 10933–10938.
- Bundeleva, I.A., Ménez, B., Auge, T., Bodenau, F., Recham, N., Guyot, F., 2014a. Effect of cyanobacteria *Synechococcus* PCC 7942 on carbonation kinetics of olivine at 20 degrees C. *Miner. Eng.* 59, 2–11. <https://doi.org/10.1016/j.mineng.2014.01.019>.
- Bundeleva, I.A., Shirokova, L.S., Pokrovsky, O.S., Bénéth, P., Ménez, B., Gérard, E., Balor, S., 2014b. Experimental modeling of calcium carbonate precipitation by cyanobacterium *Gloeocapsa* sp. *Chem. Geol.* 374–375, 44–60.
- Cam, N., Benzerara, K., Georgelin, T., Jaber, M., Lambert, J.F., Poinot, M., Skouri-Panet, F., Moreira, D., López-García, P., Raimbault, E., Cordier, L., Jézéquel, D., 2018. Cyanobacterial formation of intracellular Ca-carbonates in undersaturated solutions. *Geobiology* 16, 49–61.
- Dhami, N.K., Reddy, M.S., Mukherjee, A., 2014. Synergetic role of bacterial urease and carbonic anhydrase in carbonate mineralization. *Appl. Biochem. Biotechnol.* 172 (5), 2552–2561.
- Dittrich, M., Obst, M., 2004. Are picoplankton responsible for calcite precipitation in lakes? *Ambio* 33, 559–564.
- Dittrich, M., Müller, B., Mavrocordatos, D., Wehrli, B., 2003. Induced calcite precipitation by cyanobacterium *Synechococcus*. *Acta Hydrochim. Hydrobiol.* 31, 162–169.
- Dittrich, M., Kurz, P., Wehrli, B., 2004. The role of autotrophic picocyanobacteria in calcite precipitation in an oligotrophic lake. *Geomicrobiol. J.* 21, 45–53.
- Douglas, S., Beveridge, T.J., 1998. Mineral formation by bacteria in natural microbial communities. *FEMS Microbiol. Ecol.* 26, 79–88.
- Dupraz, C., Reid, R.P., Braissant, O., Decho, A.W., Norman, R.S., Visscher, P.T., 2009. Processes of carbonate precipitation in modern microbial mats. *Earth Sci. Rev.* 96 (3), 141–162.
- Gautier, Q., Bénéth, P., Mavromatis, V., Schott, J., 2014. Hydromagnesite solubility product and growth kinetics in aqueous solution from 25 to 75°C. *Geochim. Cosmochim. Acta* 138, 1–20.
- Guibaud, G., Bords, F., Saaid, A., D'azac, P., Van Hullebusch, E., 2008. Effect of pH on cadmium and lead binding by extracellular polymeric substances (EPS) extracted from environmental bacterial strains. *Colloid Surface B* 63, 48–54.
- Harrison, A.L., Mavromatis, V., Oelkers, E.H., Bénéth, P., 2019. Solubility of the hydrated Mg-carbonates nesquehonite and dypingite from 5 to 35°C: Implications for CO₂ storage and the relative stability of Mg-carbonates. *Chem. Geol.* 504, 123–135.
- Harrison, A.L., Bénéth, P., Schott, J., Oelkers, E.H., Mavromatis, V., 2021. Magnesium and carbon isotope fractionation during hydrated Mg-carbonate mineral phase transformations. *Geochim. Cosmochim. Acta* 293, 507–524. <https://doi.org/10.1016/j.gca.2020.10.028>.
- He, W., Zhang, L., Liu, H., Zhang, Y., Fu, B., Zhang, X., Juang, Q., 2022. CO₂ sequestration mediated by wollastonite in anaerobic digestion of sewage sludge: from sequence batch to semi-continuous operation. *Chemosphere* 287 (3). <https://doi.org/10.1016/j.chemosphere.2021.132095>. Art No 132095.
- Hopkinson, L., Kristovab, P., Ruttb, K., Cressey, G., 2012. Phase transitions in the system MgO–CO₂–H₂O during CO₂ degassing of Mg-bearing solutions. *Geochim. Cosmochim. Acta* 76, 1–13.
- Jansson, C., Northen, T., 2010. Calcifying cyanobacteria—the potential of biomineralization for carbon capture and storage. *Curr. Opin. Biotech.* 21, 365–371.
- Kantar, C., Demiray, H., Dogan, N.M., Dodge, C.J., 2011. Role of microbial exopolymeric substances (EPS) on chromium sorption and transport in heterogeneous subsurface soils: I. Cr(III) complexation with EPS in aqueous solution. *Chemosphere* 82, 1489–1495.
- Kelemen, P.B., Matter, J., Streit, E.E., Rudge, J.F., Curry, W.B., Blusztajn, J., 2011. Rates and mechanisms of mineral carbonation in peridotite: natural processes and recipes for enhanced, in situ CO₂ capture and storage. *Annu. Rev. Earth Pl. Sc.* 39, 545–576.
- Lamérand, C., Shirokova, L.S., Bénéth, P., Rols, J.L., Pokrovsky, O.S., 2020. Olivine dissolution and hydrous Mg carbonate and silicate precipitation in the presence of microbial consortium of photo-autotrophic and heterotrophic bacteria. *Geochim. Cosmochim. Acta* 268, 123–141.
- Lee, B.D., Apel, W.A., Walton, M.R., 2004. Screening of cyanobacterial species for calcification. *Biotechnol. Prog.* 20, 1345–1351.
- Lee, B.D., Apel, W.A., Walton, M.R., 2006. Calcium carbonate formation by *Synechococcus* sp. strain PCC 8806 and *Synechococcus* sp. strain PCC 8807. *Bioresour. Technol.* 97, 2427–2434.
- Ludwig, R., Al-Horani, F., de Beer, D., Jonkers, H.M., 2005. Photosynthesis-controlled calcification in hypersaline microbial mat. *Limnol. Oceanogr.* 50, 1836–1843.

- Martinez, R.E., Gardés, E., Pokrovsky, O.S., Schott, J., Oelkers, E.H., 2010. Do photosynthetic bacteria have a protective mechanism against carbonate precipitation at their surfaces? *Geochim. Cosmochim. Acta* 74, 1329–1337.
- Martinez, R.E., Weber, S., Grimm, C., 2016. Effects of freshwater *Synechococcus* sp. cyanobacteria pH buffering on CaCO₃ precipitation: implications for CO₂ sequestration. *Appl. Geochem.* 75, 76–89.
- Matter, J.M., Kelemen, P.B., 2009. Permanent storage of carbon dioxide in geological reservoirs by mineral carbonation. *Nat. Geosci.* 2, 837–841.
- Matter, J.M., Broecker, W.S., Stute, M., Gislason, S.R., Oelkers, E.H., Stefansson, A., Wolff-Boenisch, D., Gunnlaugsson, E., Björnsson, G.A., 2009. Permanent carbon dioxide storage into basalt: the CarbFix pilot Project, Iceland. *Energy Procedia* 1 (1), 3641–3646.
- Mavromatis, V., Pearce, C.R., Shirokova, L.S., Bundeleva, I.A., Pokrovsky, O.S., Bénéth, P., Oelkers, E.H., 2012. Magnesium isotope fractionation during hydrous magnesium carbonate precipitation with and without cyanobacteria. *Geochim. Cosmochim. Acta* 76, 161–174.
- McCutcheon, J., Southam, G., 2018. Advanced biofilm staining techniques for TEM and SEM in geomicrobiology: Implications for visualizing EPS architecture, mineral nucleation, and microfossil generation. *Chemical Geol.* 498, 115–127.
- McCutcheon, J., Power, I.M., Harrison, A.L., Dipple, G.M., Southam, G., 2014. A greenhouse-scale photosynthetic microbial bioreactor for carbon sequestration in magnesium carbonate minerals. *Environ. Sci. Technol.* 48, 9142–9151.
- McCutcheon, J., Dipple, G.M., Wilson, S.A., Southam, G., 2015. Production of magnesium-rich solutions by acid leaching of chrysotile: a precursor to field-scale deployment of microbially enabled carbonate mineral precipitation. *Chemical Geol.* 413, 119–131.
- McCutcheon, J., Wilson, S.A., Southam, G., 2016. Microbially accelerated carbonate mineral precipitation as a strategy for in situ carbon sequestration and rehabilitation of asbestos mine sites. *Environ. Sci. Technol.* 50, 1419–1427.
- McCutcheon, J., Turvey, C.C., Wilson, S.A., Hamilton, J.L., Southam, G., 2017. Experimental deployment of microbial mineral carbonation at an asbestos mine: potential applications to carbon storage and tailings stabilization. *Minerals* 7, 191. <https://doi.org/10.3390/min7100191>.
- McCutcheon, J., Power, I.M., Shuster, J., Harrison, A.L., Dipple, G.M., Southam, G., 2019. Carbon sequestration in biogenic magnesite and other magnesium carbonate minerals. *Environ. Sci. Technol.* 53, 3225–3237.
- Miller, A.G., Espie, G.S., Canvin, D.T., 1990. Physiological aspects of CO₂ and HCO₃⁻ transport by cyanobacteria: a review. *Can. J. Botany* 68, 1291–1302.
- Millero, F., Huang, F., Graham, T., Pierrot, D., 2007. The dissociation of carbonic acid in NaCl solutions as a function of concentration and temperature. *Geochim. Cosmochim. Acta* 71, 46–55.
- Mittelch, A.C., Dideriksen, K., Spangler, L.H., Cunningham, A.B., Gerlach, R., 2010. Microbially enhanced carbon capture and storage by mineral-trapping and solubility-trapping. *Environ. Sci. Technol.* 44 (13), 5270–5276.
- Naveed, M., Duan, J., Uddin, S., Suleman, M., Hui, Y., Li, H., 2020. Application of microbially induced calcium carbonate precipitation with urea hydrolysis to improve the mechanical properties of soil. *Ecol. Eng.* 153 <https://doi.org/10.1016/j.ecoleng.2020.105885>. Art no 105885.
- Nutman, A.P., Bennett, V.C., Friend, C.R.L., Van Kranendonk, M.J., Chivas, A.R., 2016. Rapid emergence of life shown by discovery of 3,700-million-year-old microbial structures. *Nature* 537, 535–538.
- Oelkers, E.H., Gislason, S.R., Matter, J., 2008. Mineral carbonation of CO₂. *Elements* 4, 333–337.
- Pace, A., Bourillot, R., Bouton, A., Vennin, E., Galaup, S., Bundeleva, I., Patrier, P., Dupraz, C., Thomazo, C., Sansjofre, P., Yokoyama, Y., Franceschi, M., Anguy, Y., Pigot, L., Virgone, A., Visscher, P.T., 2016. Microbial and diagenetic steps leading to the mineralisation of Great Salt Lake microbialites. *Sci. Rep.* 6, 31495.
- Pace, A., Bourillot, R., Bouton, A., Vennin, E., Braissant, O., Dupraz, C., Duteil, T., Bundeleva, I., Patrier, P., Galaup, S., Yokoyama, Y., Franceschi, M., Virgone, A., Visscher, P.T., 2018. Formation of stromatolite lamina at the interface of oxygenic-anoxic photosynthesis. *Geobiology* 16, 378–398.
- Palmer, D.A., Wesolowski, D.J., 1997. Potentiometric measurements of the first hydrolysis quotient of magnesium (II) to 250°C and 5 molal ionic strength (NaCl). *J. Solut. Chem.* 26, 217–232.
- Pan, S.Y., Chiang, P.C., Pan, W., Kim, H., 2018. Advances in state-of-art valorization technologies for captured CO₂ towards sustainable carbon cycle. *Critical Rev. Environ. Sci. Technol.* 48 (5), 471–534.
- Parkhurst, D.L., Appelo, C.A.J., 1999. User's guide to PHREEQC (Version 2)—a computer program for speciation, batch-reaction, one-dimensional transport, and inverse geochemical calculations. In: U.S. Geological Survey Water-Resources Investigations Report 99-4259 (312 pp).
- Peuble, S., Andreani, M., Godard, M., Gouze, P., Barou, F., Van de Moortele, B., Mainprice, D., Reynard, B., 2015. Carbonate mineralization in percolated olivine aggregates: linking effects of crystallographic orientation and fluid flow. *Am. Mineral.* 100, 474–482.
- Pires, J.C.M., Alvin-Ferraz, M.C.M., Martins, F.G., Simoes, M., 2012. Carbon dioxide capture from flue gases using microalgae: Engineering aspects and biorefinery concept. *Renew. Sust. Energy Rev.* 16 (5), 3043–3053.
- Plee, K., Pacton, M., Ariztegui, D., 2010. Discriminating the role of photosynthetic and hetero-trophic microbes triggering low-Mg calcite precipitation in freshwater biofilms (Lake Geneva, Switzerland). *Geomicrobiol. J.* 27, 391–399.
- Pokrovsky, O.S., Savenko, V.S., 1995. Experimental modeling of CaCO₃ precipitation at the conditions of photosynthesis in seawater. *Oceanology* 35 (N6), 805–810.
- Power, I.M., Wilson, S.A., Thom, J.M., Dipple, G.M., Gabites, J.E., Southam, G., 2009. The hydromagnesite playas of Atlin, British Columbia, Canada: a biogeochemical model for CO₂ sequestration. *Chem. Geol.* 260, 286–300.
- Power, I.M., Wilson, S.A., Small, D.P., Dipple, G.M., Wan, W., Southam, G., 2011. Microbially mediated mineral carbonation: roles of phototrophy and heterotrophy. *Environ. Sci. Technol.* 45 (20), 9061–9068.
- Priester, J.H., Olson, S.G., Webb, S.M., Neu, M.P., Hersman, L.E., Holden, P.A., 2006. Enhanced copolymer production and chromium mobilization in *Pseudomonas putida* unsaturated biofilms. *Appl. Environ. Microbiol.* 72, 1988–1996.
- Revsbech, N.P., Jørgensen, B.B., Blackburn, T.H., Cohen, Y., 1983. Microelectrode studies of the photosynthesis and O₂, H₂S, and pH profiles of a microbial mat. *Limnol. Oceanogr.* 28, 1062–1074.
- Saneiyan, S., Ntarlagianni, D., Ohan, J., Lee, J., Colwell, F., Burns, S., 2019. Induced polarization as a monitoring tool for in-situ microbial induced carbonate precipitation (MICP) processes. *Ecol. Eng.* 127, 36–47.
- Shirokova, L.S., Bénéth, P., Pokrovsky, O.S., Gerard, E., Ménez, B., Alfredsson, H., 2012. Effect of the heterotrophic bacterium *Pseudomonas reactans* on olivine dissolution kinetics and implications for CO₂ storage in basalts. *Geochim. Cosmochim. Acta* 80, 30–50.
- Shirokova, L.S., Mavromatis, V., Bundeleva, I.A., Pokrovsky, O.S., Bénéth, P., Gérard, E., Pearce, C.R., Oelkers, E.H., 2013. Using Mg isotopes to trace cyanobacterially mediated magnesium carbonate precipitation in alkaline lakes. *Aquat. Geochem.* 19, 1–24.
- Sissmann, O., Daval, D., Brunet, F., Guyot, F., Verlaquet, A., Pinquier, Y., Findling, N., Martinez, I., 2013. The deleterious effect of secondary phases on olivine carbonation yield: Insight from time-resolved aqueous-fluid sampling and FIB-TEM characterization. *Chem. Geol.* 357, 186–202.
- Stanier, R.Y., Deruelles, J., Rippka, R., Herdman, M., Waterbury, J.B., 1979. Generic assignments, strain histories and properties of pure cultures of cyanobacteria. *Microbiology* 111, 1–61.
- Stefansson, A., Bénéth, P., Schott, J., 2013. Carbonic acid ionization and the stability of sodium bicarbonate and carbonate ion pairs to 200°C— a potentiometric and spectrophotometric study. *Geochim. Cosmochim. Acta* 120, 600–611.
- Stefansson, A., Bénéth, P., Schott, J., 2014. Potentiometric and spectrophotometric study of the stability of magnesium carbonate and bicarbonate ion pairs to 150°C and aqueous inorganic carbon speciation and magnesite solubility. *Geochim. Cosmochim. Acta* 138, 21–31.
- Strickland, J.D.H., 1952. The preparation and properties of silicomolybdic Acid. I. the properties of alpha silicomolybdic acid. *J. Am. Chem. Soc.* 74 (4), 862–867. <https://doi.org/10.1021/ja01124a002>.
- Sun, X., Alcalde, J., Gomez-Rivas, E., Struth, L., Johnson, G., Travé, A., 2020. Appraisal of CO₂ storage potential in compressional hydrocarbon-bearing basins: Global assessment and case study in the Sichuan Basin (China). *Geoscience Front.* 11, 2309–2321.
- Zhu, T., Paulo, C., Merroun, M.L., Ditttrich, M., 2015. Potential application of biomineralization by *Synechococcus* PCC8806 for concrete restoration. *Ecol. Eng.* 82, 459–468.
- Zhu, T., Lin, Y., Lu, X., Ditttrich, M., 2018. Assessment of cyanobacterial species for carbonate precipitation on mortar surface under different conditions. *Ecol. Eng.* 120, 154–163. <https://doi.org/10.1016/j.ecoleng.2015.05.017>.
- Zhuang, D., Yan, H., Tucker, M.E., Zhao, H., Han, Z., Zhao, Y., Sun, B., Li, D., Pan, J., Zhao, Y., Meng, R., Shan, G., Zhang, X., Tang, R., 2018. Calcite precipitation induced by *Bacillus cereus* MRR2 cultured at different Ca²⁺ concentrations: further insights into biotic and abiotic calcite. *Chem. Geol.* 500, 64–87.